2

Macropores in p-Type Silicon

J.-N. Chazalviel and F. Ozanam
Laboratoire de Physique de la Matière Condensée, CNRS-Ecole Polytechnique, Palaiseau, France
E-mail: jean-noel.chazalviel@polytechnique.fr

2.1. INTRODUCTION

Anodization of moderately doped ($N_A \sim 10^{15}$–10^{16} cm^{-3}) p-Si substrates in aqueous or ethanolic HF has long been the most popular method for obtaining good quality microporous silicon [1,2]. The obtained material, exhibiting rather uniform porosity with pore sizes down to the nanometre range, has been the subject of many studies, most of them in the last 10 years being aimed at the understanding of its luminescence properties. Although the formation mechanism of microporous silicon is still a matter of debate, its fabrication can be controlled to a high degree of reproducibility. However, this homogeneous material is actually obtained in a limited doping range of the p-Si substrate, say between 0.1 and a few Ω cm. For highly doped Si (p^+), more complex morphologies are obtained, consisting of mesopores growing along the direction parallel to the current lines, with microporous material in between. On the other hand, it had been noted by early workers that a less controlled material is obtained if the resistivity of the starting p-Si is above a few Ω cm. Blackish layers were then observed instead of the coloured films usually obtained with "good" microporous silicon.

More detailed studies have been performed since the mid-1990s. Wehrspohn *et al.* noted that, when porous silicon is prepared from glow-discharge amorphous-hydrogenated silicon (a high-resistivity material), only a very thin layer of microporous material can be formed [3]. When the thickness of the microporous layer reaches a critical value, macropores start growing until they short-circuit the amorphous silicon film. This observation was rationalized in terms of a Laplacian instability: At the interface between two media of different resistivities, the electric current tends to concentrate near the protrusions of the lower resistivity medium. Since the resistivity of hydrogenated amorphous

silicon falls in the range 10^4–10^6 Ω cm, the electrolyte is much less resistive than the electrode. This makes the front of the microporous layer unstable on a large scale [3]. Similar growth of macropores was demonstrated by the same authors on highly resistive p-type crystalline silicon, seemingly supporting this simple resistivity argument [4]. However, further investigations by Lehmann and Rönnebeck [5] showed that things are not that simple. Whilst the formation of macropores does cease for substrate resistivities below a critical value, this value does not match the electrolyte resistivity. In parallel, studies in non-aqueous electrolytes were developed by the groups of Kohl [6,7] and Levy-Clément [8–10], and later pursued by the group of Föll [11–14]. Their results show that the interface chemistry plays an important role in orienting the morphology of the porous layer. Here again the resistivity argument appears exceedingly simple, and alternate effects were invoked.

In the following, we will first attempt to summarize the experimental observations and extract the major trends from them. In a second step, we will present the theoretical ideas put forward by the various groups. These ideas will be discussed in the third part. Finally, we will discuss the possibility to form ordered macropore arrays in the light of some recent publications.

2.2. PHENOMENOLOGY

In the following presentation, we will distinguish the macroporous structures formed in aqueous HF and those obtained in non-aqueous solvents. Among the former ones, we will include those obtained in ethanolic medium, since ethanol is just used as a surfactant, and the so-called ethanolic media are still mostly aqueous. However, we should also keep in mind that the electrolytes made from non-aqueous solvents often include significant amounts of water incorporated with the hydrofluoric acid, so that the boundary between aqueous and non-aqueous media is not really clear cut. We will nevertheless stick to it for the ease of presentation.

2.2.1. Macropore Formation in Aqueous (and Ethanolic) HF Electrolytes

Macropores are obtained in aqueous electrolytes for p-Si resistivities above a critical value, on the order of a few Ω cm. This occurs essentially in the same range of current densities as that leading to microporous-silicon formation. These conditions are recalled in Figure 2.1. Porous silicon is formed in the rising part of the current–potential curve. When current density reaches a critical value J_c, the surface becomes covered with an oxide film [15], and electropolishing takes place. The value of J_c increases with increasing concentration of HF in the electrolyte [16–21], but it also depends on solution stirring [17,19–21], temperature [18,21] and crystallographic orientation of the silicon substrate [16,18]. When anodization is carried out at a fixed current density $J < J_c$ without a prepatterning of the Si surface, microporous silicon is formed first. Macropores appear when the thickness of the microporous layer exceeds a few micrometres. This preliminary stage is sometimes referred to as the nucleation stage (though micropores and mesopores are already present at a much earlier stage). For dilute HF electrolytes or prolonged anodization times, this microporous nucleation layer is sometimes not observed on the

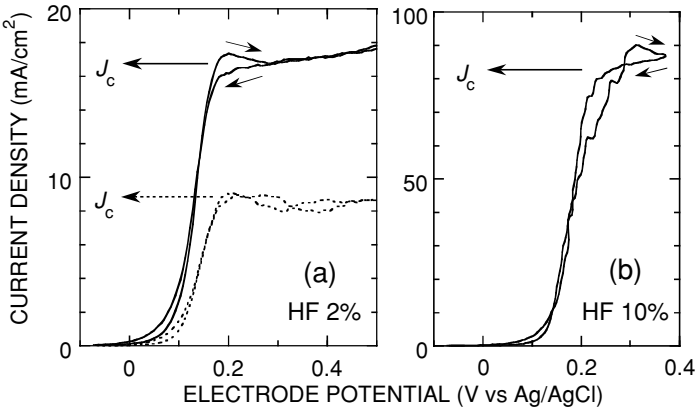

FIGURE 2.1. Voltammograms of p-Si (111) in typical aqueous HF electrolytes: (a) 2% HF (HF:H_2O:ethanol 2:68:30 (solid line) and 2:98:0 (dotted line)) and (b) 10% HF (HF:H_2O:ethanol 10:60:30). The potential scale has been corrected for ohmic drop in the silicon and the electrolyte. Recorded on a rotating disc electrode. Rotation rate 300 rpm. Temperature 18 °C. The fluctuations are due to the formation of bubbles at the electrode surface. The electropolishing current J_c is seen to increase with increasing HF concentration, but it also depends on ethanol concentration, temperature, and stirring of the electrolyte (or electrode rotation rate).

obtained samples. This is clearly due to its chemical dissolution while the macroporous layer thickens. Using short anodization times shows that it is always present at the beginning of the anodization.

2.2.1.1. Current-Line-Driven Pores and Crystallography-Driven Pores. Observation of the morphologies obtained reveals that there are two rather distinct classes of macropores, as can be seen from Figure 2.2.

- Macropores of the first class exhibit rounded bottoms and somewhat meandering walls. Their average orientation is normal to the sample surface, irrespective of the crystal orientation, and they exhibit smooth bending near the edge of the anodized area. These macropores actually appear to be filled with microporous silicon.
- On the opposite, macropores of the second class tend to form (111) facets at their bottoms and to have (110)-oriented walls. In cross section, they exhibit a more or less rounded square shape when grown along (100), and a more or less rounded triangular shape when grown along (111). No silicon is left in these pores when they form, except possibly for some microporous silicon coating their walls. For these pores, the (100) direction appears as a preferred growth direction: growth occurs along (100) even if the surface is oriented at some angle from that direction. However, the preference for (100) appears less marked than in the case of macroporous n-Si. Also, if the substrate is not free from mechanical damage, these pores may grow preferentially along dislocations lines.

These two kinds of pores are sometimes referred to as "current-line-driven pores" and "crystallography-driven pores", respectively, and we will adopt these terms in the following. For a given electrolyte composition and a given silicon doping, a transition

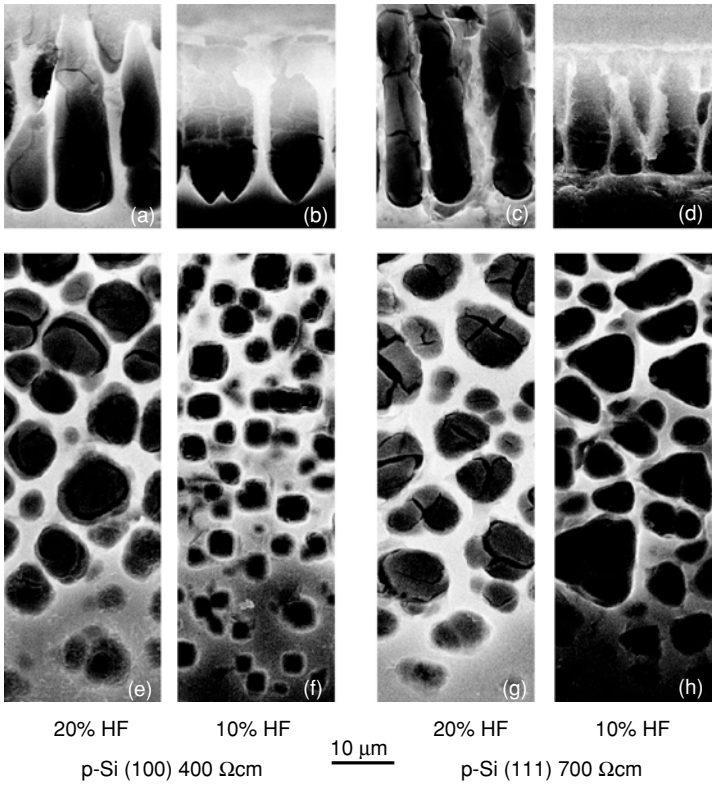

FIGURE 2.2. Crystallography-driven pores versus current-line-driven pores. Side views (a–d) and top views on a bevelled edge near the pore bottoms (e–h) of macropores formed on p-Si at a current density of 30 mA/cm^2 (anodization time 20 minutes), in various experimental conditions, indicated at the bottom of the figure. Note the porous-silicon filling and the rounded shape of current-line-driven pores (a, e, c, g), and the change in shape of crystallography-driven pores depending on the orientation of the surface (squared shape on (100) (b, f) and triangular shape on (111) (d, h)).

from current-line-driven pores to crystallography-driven pores is observed as current density is increased. There seems to be more or less agreement among the groups that crystallography-driven pores are obtained when the pore bottoms are under electropolishing conditions. The known variation of the electropolishing current density as a function of surface orientation [16,18] would then explain the anisotropy of pore growth. However, though this interpretation is plausible, there is as yet no quantitative proof of the relationship between the two phenomena, nor is it clear whether the moderate anisotropy of the electropolishing current is sufficient to account for the sharp angles observed in the pore shape.

When current density is further increased, pore formation stops, and a wavy surface is formed instead. Surprisingly, Lehmann and Rönnebeck have reported that this change of regime occurs for a current significantly smaller than the nominal value of the electropolishing plateau [5]. However, this limit is accessible only in electrolytes with a rather low HF concentration, where chemical dissolution of silicon is non-negligible,

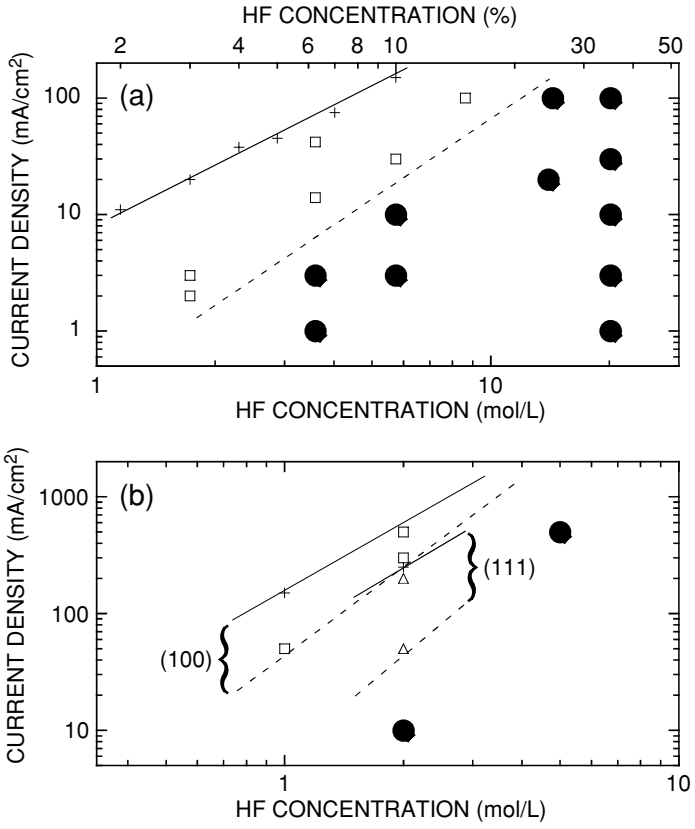

FIGURE 2.3. Morphological map of macropores on p-Si: (a) in aqueous (ethanolic) HF electrolyte and (b) in acetonitrile electrolyte (with 2.4 M H_2O). The crosses and the solid lines represent the electropolishing regime. The regime of current-line-driven pores (black circles) and that of crystallography-driven pores (squares for (100), triangles for (111)) are separated by a dashed line. The data in (a) are for (100) orientation. Note the difference between (100) and (111) in (b). Data are taken from [5,8,9,22,23].

and HF depletion at the pore bottoms may be important. We then regard as plausible that in this regime a highly porous structure is actually formed, but its slow chemical dissolution or mechanical breaking may be responsible for the mismatch in the current densities. Figure 2.3a summarizes results collected from various sources [5,22,23], giving a map of the two morphological regimes in the HF concentration/current-density plane.

2.2.1.2. Characteristic Sizes. The characteristic sizes of the macroporous structure, that is, the average pore diameter and wall thickness, both increase with increasing silicon resistivity, spanning a typical range from 1 μm to 10 μm, as the resistivity is increased from 10 Ω cm to 1000 Ω cm and above. The two quantities vary about proportionally to $\rho^{1/2}$, where ρ is silicon resistivity. As said above, for resistivities below a few Ω cm, there is no longer formation of a macrostructure, but rather a uniform

micro(meso)porous layer grows steadily, up to thicknesses as large as a few hundred micrometres.

The growth rate of the macropores is about the same as that of microporous silicon. Especially, it is about proportional to the applied current density [5]. This feature stands in contrast to macropore growth on n-Si, which occurs at a constant rate, set by the value of the electropolishing current density. The fact that macropores on p-Si can grow much more slowly than on n-Si clearly indicates that current density at the pore bottoms may be much smaller for p-Si than for n-Si. This is especially true in the regime of current-line-driven pores.

2.2.2. Macropore Formation in Non-Aqueous Electrolytes

It is a common rule that the electrochemical behaviour of an electrode in a non-aqueous electrolyte is often governed by the small amount of water present in that electrolyte. Formation of porous silicon in non-aqueous electrolytes seems indeed to follow that rule. It seems that the only investigations on the behaviour of silicon in anhydrous HF electrolytes were made by the group of Kohl [6,7], using acetonitrile (ACN) as the solvent. For p-type silicon, the results were that no microporous silicon is ever formed. For (100) orientation, crystallography-driven macropores were obtained. On (111), only pyramidal etch pits were observed. However, if some water is present in the organic electrolyte, behaviours reminiscent of those observed in aqueous HF appear. Many of such experiments have been made in various solvents, the most used ones being ACN, propylene carbonate (PC), dimethylsulfoxide (DMSO) and dimethylformamide (DMF).

Among those solvents, ACN is probably the best documented case. In anhydrous ACN + HF solutions, the voltammogram of p-Si exhibits a continuous rise [6], without any limitation such as the electropolishing plateau of Figure 2.1. However, in the presence of water, such a limitation appears, due to the formation of an oxide when the current density reaches a critical value [6,8]. In such electrolytes, a microporous nucleation layer is formed, just as in aqueous electrolytes. When the current density is increased, the same morphology sequence as in aqueous electrolytes is observed: current-line-driven macropores (filled with microporous silicon), then crystallography-driven macropores and finally electropolishing. A map of the morphological regimes may be drawn from the few data available in the literature, and is shown as Figure 2.3b, here for a water concentration of 2.4 M [8]. Note the similarity with Figure 2.3a, except that the boundaries between the different regimes occur at lower HF concentration and/or higher current densities than in the case of aqueous electrolytes. The average diameter of the macropores and the average wall thickness have been found to exhibit a slight decrease upon increasing current density [8] (though the observed increase in pore size with increasing porous-layer thickness makes it difficult to extract a single figure for the average pore diameter). Adding increasing amounts of water to the electrolyte results in an increase of pore diameter, and may ultimately result in electropolishing, because the electropolishing current density J_c decreases as a function of water concentration in the H_2O/ACN mixtures (a similar variation of J_c is observed for H_2O/ethanol mixtures, as can be seen from Figure 2.1a). Finally, it was found that, as in the case of aqueous electrolytes, macropores can be obtained only for p-Si resistivities above a few Ω cm [8].

When other solvents are used, the characteristic sizes of the porous structure appear to depend on the solvent to a rather weak extent (see Table 2.1 of [10]). However, the morphological maps exhibit significant variations. Whilst using PC leads to results closely similar to those obtained with ACN, a wider range for crystallography-driven pores is observed when using DMF and DMSO [9,10,13,14]. For these solvents, macropores can be formed down to very small current densities, and the crystallographic effects appear strongly enhanced: not only do the pore bottoms exhibit (111) facets, but the preference for the (100) growth direction is so strong that (100)-oriented pores are obtained even when starting from a (111) Si surface (see Figure 2.4) [13,14]. To a lesser extent, the (113) directions also appear as preferred growth directions (see Figure 2.4) [13,14]. These features, reminiscent of those observed for n-Si, are observed for p-Si

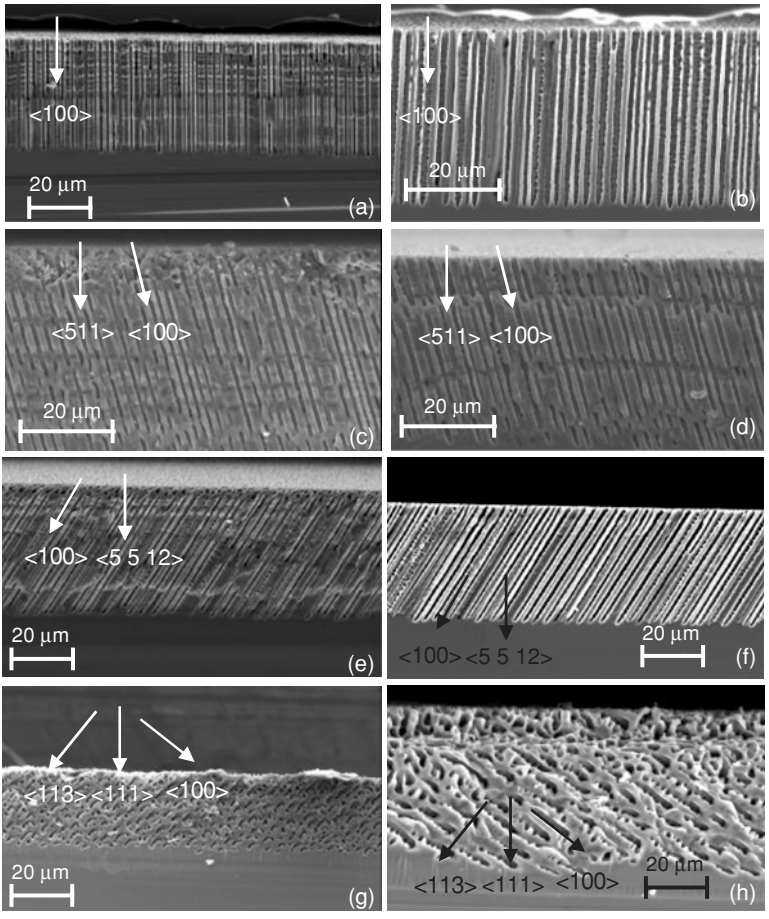

FIGURE 2.4. Crystallography-driven pores obtained in non-aqueous HF electrolytes (after [14]). DMSO + 4% H_2O + 4% HF (a, c, e, g) and DMF + 4% H_2O + 4% HF (b, d, f, h). p-Si resistivity 10–20 Ω cm. Current density 2 mA/cm^2. Note the marked preference for ⟨100⟩ and ⟨113⟩ growth directions. Reproduced by permission of the Electrochemical Society.

only in these peculiar non-aqueous solvents. Finally, in DMF and DMSO, macropores have been formed down to silicon resistivities of 0.2 Ω cm [10].

2.3. THEORY

In this section, we will try to present the various ideas that have been put forward in order to rationalize the above observations. The presentation will be organized with respect to the classes of ideas, which closely map the various different groups. The discussion section will be organized with respect to the different phenomena and systems.

2.3.1. Role of the Space Charge

Following ideas first proposed by Lehmann and Föll for macropore formation on n-Si [24], Lehmann and Rönnebeck have considered the plausible role of the space charge in the formation of macropores on p-Si [5]. The idea is that silicon dissolution is governed by the flow of holes reaching the surface. Since the surface is under weak depletion conditions, the holes have to overcome a Schottky barrier. According to Lehmann and Rönnebeck [5], the overall rate of hole transfer is limited by the diffusion velocity over the barrier. This quantity is proportional to the electric field inside the barrier, that is, inversely proportional to the barrier thickness. At the pore tips, due to interface curvature, the space-charge layer is thinner, which makes the hole diffusion velocity higher at these locations. This results in an increased dissolution rate at the pore tips. In line with these ideas, the wall thickness is expected to be determined by the thickness of the depletion layer: the maximum thickness so that a wall is fully depleted is just $2w_{SC}$, where w_{SC} is the usual depletion-layer width. However, to this point the present theory does not give a prediction on characteristic pore diameter.

2.3.2. Chemical Effects

The proposal of Lehmann and Rönnebeck allows one to understand the variation of the wall thickness with silicon doping. However, from the observation that very different morphologies may be obtained when changing the solvent, it is clear that chemical effects come into play. For example, as pointed out by Kohl *et al.* [6,7], in anhydrous ACN electrolyte, there cannot be any oxide on the Si surface, and dissolution proceeds by the formation of SiF bonds only. This argument obviously does not hold when some water is present. However, many other chemical factors may play a role.

Levy-Clément *et al.* have underlined the fact that the dissolution rate may not be limited by hole supply to the interface, in contrast to Lehmann and Rönnebeck's assumption, but also by interface kinetics. When one writes the chemical steps of the Si dissolution, it is clear that the intermediate species may interact with the solvent, and the rates of each step may depend on the polar character of the solvent, its ability to solvate nucleophilic anions and the solubility of the dissolution products [10]. Furthermore, the band bending, which plays a key role in Lehmann and Rönnebeck's approach, may be solvent dependent: for different solvents, the applied potential may divide in different ways between the semiconductor space charge and the Helmholtz layer. An interesting point is

that DMF and DMSO, which allow to grow spectacular crystallography-driven pores, belong to the same class of aprotic protophilic solvents [10]. However, the relationship between these two experimental facts is not yet clear.

On the other hand, the group of Föll has addressed the question of anisotropic pore growth in more detail, and has proposed a new model, which among other results may account for these effects. The model rests on the hypothesis that, on a local scale, dissolution takes place through cyclic "current bursts" [25]. A cycle begins with a current increase leading to local Si dissolution, then the reactants get exhausted and the surface gets oxidized. When the oxide gets thick enough, the current vanishes, the oxide dissolves, and the surface gets rehydrogenated and passivated, till a new cycle starts [25]. The hydrogen repassivation step would be that responsible for the anisotropic effects. At the core of the model is the idea of a competition between oxidation and hydrogenation, a competition that would lead to unstable behaviour on a local scale. The authors suggest that macropores can appear when there is sufficient oxidation to balance direct dissolution. Since oxidation is considered to be an isotropic process, more anisotropic pores are expected in "less oxidizing" solvents, or in circumstances where there is less oxygen and more hydrogen. As a support to their model, the authors report that adding diethyleneglycol (supplying hydrogen) to ACN makes the pores more regular [11].

2.3.3. Linear Stability Analysis (LSA) Approach

A problem with many of the above theories is that they are more qualitative than quantitative. Hence, they are rather difficult to either prove or disprove. In an attempt to make quantitative predictions, several groups have tried to use linear stability analysis (LSA) in order to assess their ideas. Linear stability analysis is a general method to study the behaviour of the interface between two phases [26]. It is used especially in the study of growth phenomena. It consists in studying the stability of a flat interface. For that purpose, a small sinewave perturbation of the flat interface is assumed, of amplitude δ and wave vector q (see Figure 2.5), and the equations of the proposed model are used to explore the time evolution of that perturbation. Since the perturbation is taken infinitely small, the equations can be linearized and the evolution problem can often be solved with a limited amount of mathematics. The evolution of δ comes out generally of the form $d\delta/dt = \beta(q) \times \delta$. If $\beta(q) < 0$, the perturbation tends to damp out exponentially: the interface is stable with respect to a perturbation of wave vector q. If $\beta(q) > 0$,

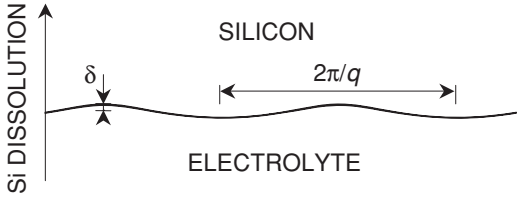

FIGURE 2.5. Principle of linear stability analysis. An initially planar interface is perturbed by a small sinewave perturbation of amplitude δ and wave vector q, and the evolution of δ as a function of time is studied.

the perturbation increases exponentially with time, until the linear approximation holds no longer. The wave vector q_{max} corresponding to the maximum value of β gives the characteristic scale of the perturbation that will appear first. Therefore, this method is a valuable tool to predict the onset of instability of an interface. However, in principle, it cannot predict its behaviour beyond the linear regime.

Linear stability analysis has been used by Kang and Jorné for the study of macroporous-silicon formation on n-Si [27], and later by Valance for the study of porous-silicon formation on n-Si and p-Si [28,29]. However, the latter results were rather at variance with the experimental data. Recently, our group has reconsidered the case of p-Si, and fair agreement was obtained [30,31,23]. Our model will be described here in some detail. It rests on the classical assumption that silicon dissolution is governed by the reaction of the first hole at the interface. Our ingredients are essentially an extension of the space-charge model, aimed at incorporating other effects, and include the following:

1. Near the maxima of the sinewave (depressions of the Si surface), the thinning of the space-charge layer results in an increase of the hole diffusion velocity $\upsilon_D = \mu E_S$, where μ is hole mobility and E_S interface electric field. This is nothing but the LSA version of Lehmann and Rönnebeck's argument [5,30].
2. At the same locations, the increased interface electric field E_S results in an increased Helmholtz potential drop [32], and a decrease in band bending (Schottky-barrier lowering), given by $\Delta\Phi_{SC} = -e\varepsilon\varepsilon_0 E_S/C_H$, where e is elementary charge, C_H is Helmholtz capacitance and $\varepsilon\varepsilon_0$ is the permittivity of silicon. This effect was not taken into account by previous investigators, especially Lehmann and Rönnebeck.
3. The reactivity of the interface is characterized by a reaction velocity υ_R, which occurs as a process in series with hole transport through the space-charge layer. Namely, the current is taken as $J = -eN_A\upsilon \exp(-\Phi_{SC}/k_BT)$, where $\upsilon^{-1} = \upsilon_D^{-1} + \upsilon_R^{-1}$, N_A is the acceptor concentration, Φ_{SC} is the band bending at the applied potential considered, T is the absolute temperature and k_B is the Boltzmann's constant. The reaction velocity υ_R is an important feature, as it bears all the chemical information in the model. It is assumed to vary with surface curvature as $\upsilon_R = \upsilon_R^0 (1 + \kappa a^2)$, where κ is curvature (taken positive for a surface protrusion) and a a characteristic interatomic length. This form provides a fair description of the higher surface reactivity at the more open positions available on a silicon protrusion, and the lower reactivity due to steric hindrance at the depressions. However, by construction it assumes direct hole transfer at the interface. Especially, it takes into account neither the possible presence of surface states nor that of an oxide layer. Therefore, it cannot apply to the electropolishing regime and cannot account for crystallographic effects.
4. On a large scale (small q), the potential distribution is affected by the resistivities of the silicon and the electrolyte.

Working out this model leads to a $\beta(q)$ function always positive in a wide range of q's. Figure 2.6 shows a typical plot of $\alpha(q) = \beta(q)/V$, where V is the average velocity of the interface (knowledge of α is equivalent to that of β, but α is more convenient here as it is homogeneous to an inverse length).

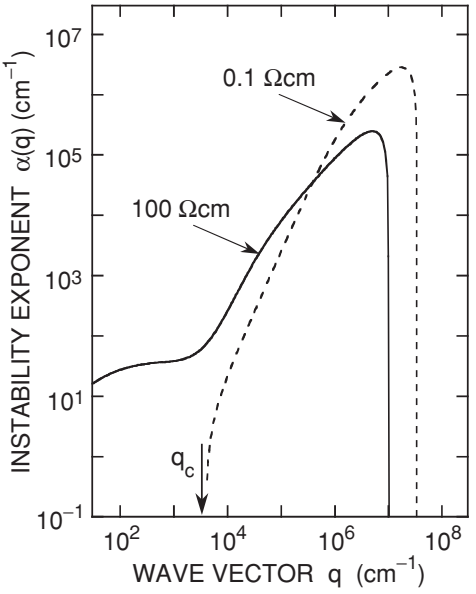

FIGURE 2.6. Typical $\alpha(q)$ curves obtained in [31]. Note that the maximum of α occurs for $1/q$ in the nanometre range, but the behaviour at small q is strongly dependent on silicon resistivity.

Near its maximum, α is approximately given by $Sq - q^2 a \upsilon_D/(\upsilon_R + \upsilon_D)$, where $S = \upsilon_R/(\upsilon_R + \upsilon_D) + e\varepsilon\varepsilon_0 E_S/k_B T C_H$ is a dimensionless parameter, on the order of 0.1–1, which arises from the destabilizing effects 1 and 2 [30]. The scale where the first instability of the interface occurs is then on the order of $1/q_{max} \sim a/S$, in the nanometre range. The model then accounts for the initial stages of the formation of microporous silicon, giving a correct order of magnitude for the scale of the structures in that material [31].

In principle, LSA does not allow one to predict what occurs beyond the linear regime. Here, however, information on the larger scales can still be obtained: when a microporous layer is formed, due to depletion of the semiconductor in the microporous structure, the physical properties of the layer are essentially those of the electrolyte inside the pores. The above LSA approach can then be used as it stands, for the study of the stability of the front of the porous layer. The existence of a wide range of q's below q_{max}, where α is positive, shows that the front will develop instabilities at increasingly large scales (q^{-1} increasing with α^{-1}, which is itself on the order of the porous-layer thickness Δ), thereby forming mesopores and macropores filled with microporous silicon.

Interestingly, depending on the relative resistivities of the semiconductor ρ_s and the electrolyte ρ_e, the range of positive α's extends down to zero q (for $\rho_s > \rho_e$) or stops at a critical value q_c (for $\rho_s < \rho_e$) (see Figure 2.6). From this result, it was earlier concluded that macropore formation is governed by the resistivity ratio ρ_e/ρ_s [3,4]. However, this conclusion was disproved by experiment [5,8–10]. As a matter of fact, an inspection of Figure 2.6 shows that the value of q_c is so low and corresponds to values of α so small

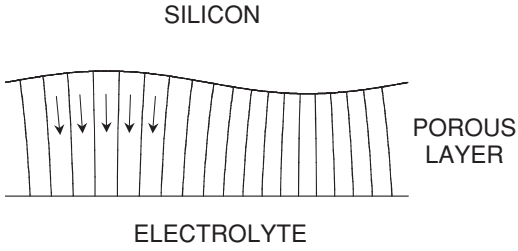

FIGURE 2.7. Stabilization of the pore front by the resistivity of the electrolyte. The pores grow in the direction perpendicular to the front. Since the pore walls are insulating, the current feeding a protruding part of the front has to flow through a narrowed region of the electrolyte, which strongly enhances the ohmic drop associated with that region.

that this regime is hardly reached in practice. In practical conditions, α values down to 10^2–10^4 cm^{-1} may be operative (depending on the porous-layer thickness $\Delta \sim \alpha^{-1}$). In this regime, the model does predict the formation of macropores of increasing size, with characteristics weakly dependent on the ρ_e/ρ_s ratio. Therefore, the actual question is not about the origin of macropores, but rather about their disappearance at low resistivities, and also about the observed morphology: why do the macropores grow parallel, rather than exhibiting a hierarchy of increasingly large pores, as would be expected from the positive value of α up to large scales? These two questions were addressed in a recent work [31,23], which is summarized hereafter.

Treating the microporous layer as an effective medium of isotropic resistivity ρ_e is not appropriate: since the walls are insulating, the preferential orientation of the pores parallel to the growth direction makes the resistivity anisotropic. Furthermore, the pores tend to grow perpendicular to the local front surface. Hence, around a protrusion of the porous layer, the increased interface area is fed by a narrower bunch of pores (see Figure 2.7). This makes the electrolyte resistivity play a much more important role than would be the case for an isotropic medium. A detailed calculation shows that a stabilizing contribution to α arises from that effect, and this contribution increases with increasing layer thickness. At early growth times, a hierarchical array of macropores is then expected, till this stabilizing contribution counterbalances the destabilizing contribution of Figure 2.6. The pores existing at this stage then continue their growth as a stable parallel array. This change of regime is predicted to occur for a characteristic size $1/q_c^*$ [23]:

$$\frac{1}{q_c^*} \approx \left[\lambda^3 S^3 \frac{k_B T}{eJ\rho_e}\right]^{1/4} \tag{2.1}$$

where λ is the ratio Φ_{SC}/eE_S (i.e., $\lambda \sim w_{SC}$). The characteristic length π/q_c^* is the characteristic pore diameter above which parallel pore growth is predicted to occur. This prediction should apply to the regime of current-line-driven macropores.

The last intriguing point is the observation that no macropores are formed below a certain resistivity of the silicon sample. A proposal can be made from the fact that, when doping increases, the average space-charge thickness decreases as $N_A^{-1/2}$, whereas the average interimpurity distance decreases as $N_A^{-1/3}$. The two quantities cross smoothly for $N_A \sim 10^{18}$ cm^{-3}, but they are pretty much of the same order of magnitude already for

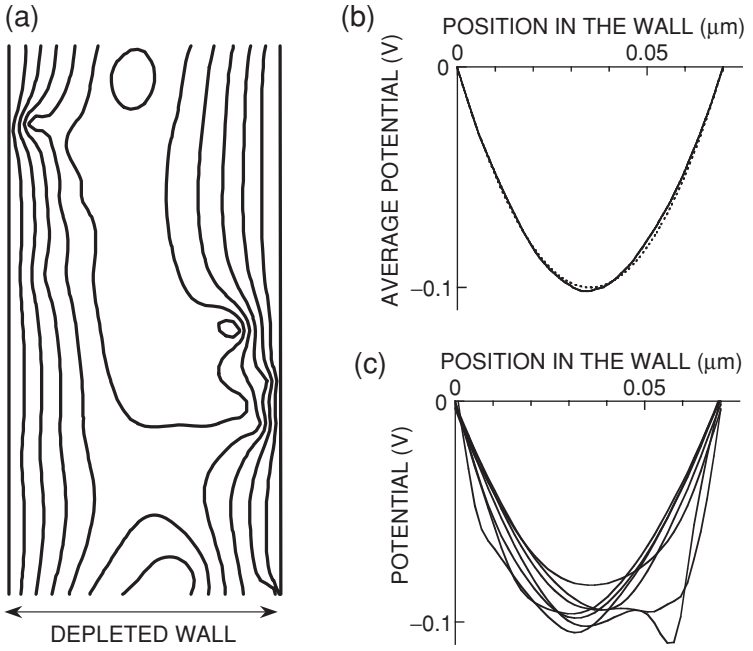

FIGURE 2.8. Fluctuation effects due to the small number of impurities in a depleted wall when doping increases. Here, simulation of a portion of depleted wall, of thickness $2w_{SC} = 0.07$ μm and surface area $4w_{SC} \times 4w_{SC}$, for a doping of 10^{17} cm^{-3} (there are 140 ionized impurities in this volume). (a) two-dimensional map in a cross section of the wall. (b) Potential averaged in the directions parallel to the wall. (c) Potential along a few straight lines perpendicular to the wall. Although the potential averaged over the directions parallel to the wall is fairly close to the classical parabolic profile (dotted line in (b)), the map of the potential in a cross section of the wall ((a) or (c)) exhibits strong deviations from this profile. This may render the wall permeable to holes, so that the assumption of an insulating wall breaks down (after [23]).

$N_A \gtrsim 10^{16}$ cm^{-3}. As a result, the number of ionized impurities when crossing a depleted wall is small, and fluctuation effects may become important, leading to conduction paths through the wall (see Figure 2.8). We have made a numerical simulation of a depleted wall with a band bending of 0.1 eV, which is the typical estimated band bending in the regime of porous-silicon formation in aqueous (ethanolic) HF. The insulating character of the wall was determined from the energy of the lowest acceptor state in a parallelepipedic portion of the wall. As fluctuation effects become important, the wall remains insulating for thicknesses smaller and smaller as compared to the naive $2w_{SC} \propto N_A^{-1/2}$ law. The conclusion is that a depleted wall can no longer remain insulating for a critical doping in excess of a few 10^{16} cm^{-3} [23]. A major consequence of the loss of this insulating character is that the anisotropy of the resistivity of the porous layer disappears, the above reasoning breaks down, and no parallel macropore growth is to be expected. As first suggested by Lehmann and Rönnebeck (though for reasons that are in our opinion incorrect), higher dopings result in the growth of a mesoporous layer. Interestingly, this critical doping is expected to strongly increase for higher band bendings [23].

2.4. DISCUSSION

Here, we will put the emphasis on the possibilities to get predictive quantitative information on characteristic pore sizes and morphologies. This will be less of a review and more of the authors' personal views. The discussion will be organized according to the two classes of pores.

2.4.1. Crystallography-Driven Pores

If we accept that crystallography-driven pores are under electropolishing conditions at their bottoms, Lehmann and Rönnebeck's ideas can be turned into quantitative predictions on characteristic pore sizes. As stated in Section 2.3.1, the average wall thickness is expected to be given by $2w_{SC}$ [5]. Now, if the current density at the pore bottoms is set to the electropolishing value J_c, one can write $P = J/J_c$, where P is porosity. This argument is similar to that given for the case of n-Si [24,18]. For a given pore geometry, there is a relationship between porosity, pore diameter and wall thickness. This relationship is not too much dependent on pore geometry. Taking either a honeycomb lattice of hexagonal pores or a square lattice of square pores, porosity is $P = [R/(R + w_{SC})]^2$, where R is pore "radius" (here apothem of the polygon). Hence, we get the pore diameter d (a slightly modified form of original Lehmann's formula) [18]:

$$d = \frac{2w_{SC}}{P^{-1/2} - 1} = \frac{2w_{SC}}{(J_c/J)^{1/2} - 1}. \tag{2.2}$$

The observed increase in wall thickness as a function of doping is in fair agreement with Lehmann and Rönnebeck's prediction. Lust and Levy-Clément have pointed out that there does not seem to be a minimum wall thickness [10]. However, this is not really surprising in view of the statistical dopant fluctuations discussed in Section 2.3.3 and the disordered macropore structure. As a matter of fact, the average (rather than minimum) wall thickness seems to match the $2w_{SC}$ prediction reasonably well. Interestingly, this prediction appears better verified on p-Si than on n-Si (where minority-carrier diffusion may lead to pore spacings well in excess of $2w_{SC}$) [5,33]. Also, the increase in pore diameter before approaching the transition to electropolishing is well accounted for by Equation (2.2). Finally, we regard as very plausible that the anisotropy of the electropolishing current bears the explanation for the anisotropy of pore shape and pore growth direction. In the detail, the difference between "anisotropy of the electropolishing current" and the model of Föll *et al.* (anisotropy of the kinetics of rehydrogenation) may be mostly a matter of vocabulary. However, anisotropy of the electropolishing current may also result from factors not taken into account in Föll's model (e.g., role of SiOH species), and the oscillatory nature of the current on the microscopic scale does not appear as a mandatory requirement for electropolishing to take place. Nevertheless, a careful study of the electropolishing current as a function of crystallographic orientation would be necessary in order to quantitatively assess the role of its anisotropy in the growth of macropores. In the detail, one may also wonder which value should be taken for J_c in Equation (2.2). For example, if pores are growing along (100) with (111) facetted bottoms, J_c should plausibly be taken as $\sqrt{3} \times J_c(111)$ rather than as $J_c(100)$, but it is not clear either whether $J_c(100)$ can actually be determined by a direct measurement.

These problems may be related to the discrepancy observed by Lehmann and Rönnebeck between the electropolishing current and that corresponding to disappearance of the macropores.

2.4.2. *Current-Line-Driven Pores*

For the case of current-line-driven pores, the space-charge argument is still operative for predicting the average wall thickness, a prediction which remains in fair agreement with observations (see Figure 2.9). However, the pore diameter can no longer be determined by the electropolishing condition, and the only available theoretical prediction is that stemming from the LSA study of the pore front (Equation (2.1)). Let us recall that the basic mechanism at work in this theory is the current limitation due to the series resistance of the electrolyte along the pores. Though the early proposed criterion on the semiconductor to electrolyte resistivity ratio has been disproved by experiment, the theory looks attractive, as it accounts for the observations on the nucleation stage and the progressive increase in pore size before reaching a steady state of parallel growth.

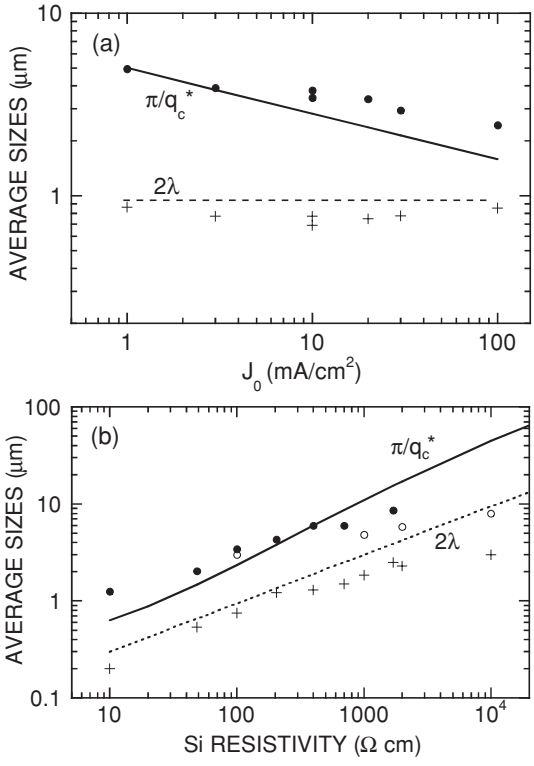

FIGURE 2.9. Comparison of characteristic macropore sizes in the current-line-driven regime, when changing current density (a) and silicon doping (b), in 35% ethanolic HF (HF:H_2O:ethanol 35:35:30 by volume), after [23]. The hollow symbols refer to data obtained in 25% ethanolic HF. The solid line is from Equation (2.1) and the dotted line is $2w_{SC}$. In (a), $\rho_e = 100\,\Omega$ cm. In (b), $J = 10$ mA/cm^2.

Furthermore, electrolyte resistivity must still play a role at large scale, especially in view of the wall depletion, which constrains the current lines inside the pores.

Figure 2.9 shows a comparison of experiment with the theoretical predictions (wall thickness given by $2w_{SC}$, and pore diameter given by Equation (2.1)), when varying current density and silicon resistivity, for a 35% ethanolic HF electrolyte. The agreement is seen to be fair. The deviations between the theory and experiment for the highest resistivities may be due to failure of the assumption that w_{SC} scales as $\rho_s^{1/2}$, since highly resistive samples are generally compensated. Figure 2.10 shows similar comparisons between theory and experiment when electrolyte composition is changed. Such changes may result in changing the reaction velocity υ_R (assumed proportional to HF concentration) and the electrolyte resistivity ρ_e (determined experimentally). Here, again the agreement is fine. Note that, for Figure 2.10a, S was adjusted due to the lack of information on Φ_{SC} and C_H in ACN (the resulting value $S = 0.85$ appearing somewhat large), but Figure 2.10b was obtained without any adjustable parameter.

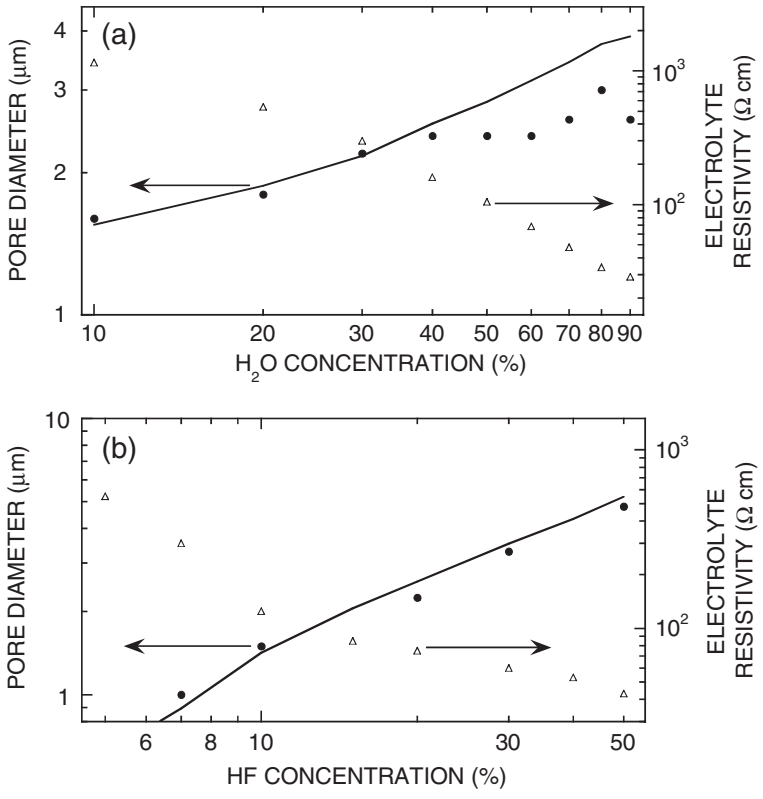

FIGURE 2.10. Comparison of characteristic macropore sizes in the current-line-driven pore regime, when changing the electrolyte. Experiment (black circles) and theory (curves) using measured electrolyte resistivity (hollow triangles). (a) Changing H_2O concentration in acetonitrile/2 M HF electrolyte. $\rho_s = 10$–$15\,\Omega$ cm, $J = 10$ mA/cm^2. Data from [8]. Theory from Equation (2.1) with $\lambda = 0.165$ μm, $S = 0.85$. (b) Changing HF concentration in mixtures HF:H_2O:ethyleneglycol x:x:$100 - 2x$. $\rho_s = 1500\,\Omega$ cm, $J = 10$ mA/cm^2. Data from [23]. Theory from Equation (2.1) with $\lambda = 1\,\mu$m, $\Phi_{SC} = 0.1$ eV (whence $\upsilon_D = 4.7\,10^5$ cm/s) and υ_R (cm/s) $= 3\,10^3 \times$ [HF%].

Finally, the observed disappearance of macropores when the resistivity of p-Si becomes lower than a few Ω cm is fairly well accounted for by the loss of the insulating character of the walls due to statistical fluctuations of the dopant concentration (see Figure 2.8). In conclusion, the theory of [23] could certainly be refined by taking into account, e.g., the possible effect of surface states, HF depletion at the pore bottoms, and quantum confinement effects [34]. However, the above facts give the feeling that the formation of current-line-driven macropores in p-Si is fairly well accounted for by that theory in its present form.

2.4.3. Morphological Map

If Equation (2.1) accounts for the average diameter of current-line-driven macropores and Equation (2.2) for that of crystallography-driven macropores, the change from current-line-driven pores to crystallography-driven pores is expected to occur when the second member of Equation (2.1) equals that of Equation (2.2). Physically, this means that the two stabilizing effects (series resistance of the macropores and electropolishing at the pore bottoms) are of comparable strength. If the two quantities in Equations (2.1) and (2.2) are plotted as a function of J (see Figure 2.11), it is seen that the two curves cross somewhere below the electropolishing current density J_c (which is an increasing function of HF concentration). At current densities lower than the crossover value, Equation (2.1) predicts a larger pore size than Equation (2.2): therefore, electropolishing at the pore bottoms is not reached, and current-line-driven pores are predicted, with a diameter of the form $AJ^{-1/4}$, where A is a constant which can be extracted from Equation (2.1). At current densities higher than the crossover value, the pore size predicted by Equation (2.1) would lead to current densities at the pore bottoms higher than the electropolishing current. Therefore, the limitation by electropolishing takes over that by the series resistance of the electrolyte, and crystallography-driven pores are expected. So, one may generally expect that crystallography-driven pores will be

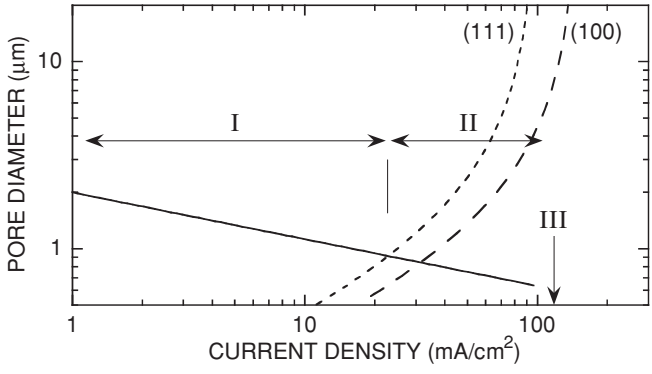

FIGURE 2.11. Predicted crossing between current-line-driven pores (Equation (2.1), solid line) and crystallography-driven pores (Equation (2.2), dotted line for (111), assuming $J_c(111) = 100$ mA/cm^2, and dashed line for (100), assuming $J_c(100) = 150$ mA/cm^2). When current is increased, one successively encounters current-line-driven pores (I), crystallography-driven pores (II), and electropolishing (III). Here, the curves have been calculated for 10% ethanolic HF (HF:H_2O:ethanol 10:50:30, $\rho_e = 20\,\Omega$ cm), and $\rho_s = 100\,\Omega$ cm. Note the fair agreement with Figure 2.3a.

observed in a limited range of current densities, just below the onset of electropolishing. In practice, this range is probably widened by the change in dissolution valence from $\sim$2 to $\sim$4 when entering the electropolishing regime [5,35,36]. Also, it will be wider if the anisotropy of the electropolishing current is larger, and/or if the prefactor A from Equation (2.1) is smaller. This may be the case if ρ_e is large and/or if S is small, which might be favoured by a small value of the reaction velocity υ_R.

At first sight, the morphologies observed for non-aqueous solvents might give the feeling that things are quite different from the case of aqueous HF [14]. However, this feeling is largely due to the fact that most data in the literature are obtained at a given current density. If the full morphological map is considered (i.e., in the HF concentration/current-density plane), there does not seem to be real qualitative differences between aqueous and non-aqueous media. In ACN, it has been observed that the boundaries between the different morphological regimes occur at a lower HF concentration and/or higher current density than in aqueous electrolytes (see Figure 2.3). This effect is clearly due to the lower water concentration and weaker probability of forming an oxide (whence a higher electropolishing current density). On the opposite, the lower electropolishing current density observed in DMF and DMSO, plausibly due to the lower solubility of fluorosilicates in these solvents, leads to a shifting of the morphological map towards the low current densities. The wider range of crystallography-driven pores observed in these solvents may be due to a stronger anisotropy of the electropolishing current, and/or to a smaller value of the prefactor in Equation (2.1).

Finally, the lower resistivity limit down to which macropores can be grown has been found to be smaller in DMF and DMSO than in water, ACN or PC. According to the theory of Section 2.3.3, this might be due to a larger value of the band bending Φ_{SC} under porous-silicon formation conditions in these solvents. Unfortunately, there is as yet no published determination of Φ_{SC} in these systems. However, for anodization in an aqueous electrolyte, it has been reported that addition of a cationic surfactant improves the "quality" of the pores dramatically, whereas addition of an anionic or a neutral surfactant has no effect or even detrimental effects [37]. Adsorption of cationic species is expected to shift the flatband potential positively, that is, to increase the band bending at the p-Si/electrolyte interface. One may then infer that the beneficial effect of a cationic surfactant is indeed related to such an increase of the band bending, which further supports the theory of [23].

2.5. ORDERED MACROPORE ARRAYS

Formation of ordered macropore arrays has long been a tantalizing goal, in view of the possible applications to the fabrication of microstructures for electronic, micromechanical or optical applications. Crystallography-driven pores appear as the best choice for realizing regular structures, since their growth is controlled by the crystallographic directions and may therefore be perfectly rectilinear. However, a perfectly regular array will not tend to form spontaneously: the pores exhibit short-range order but no spontaneous long-range ordering. Rather, the mechanism of stabilization by the resistivity of the electrolyte tends to make the pores grow with the same cross section as they started. For obtaining regular arrays, prepatterning is then necessary.

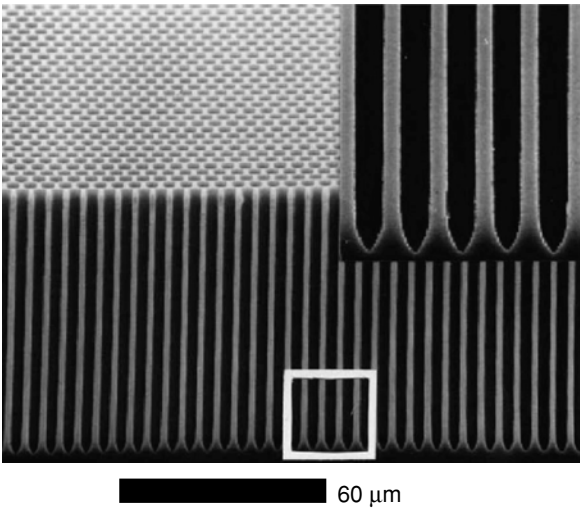

FIGURE 2.12. Example of a regular array of macropores grown by Chao *et al.* [37]. p-Si (100) 13 Ω cm. Ethanolic HF electrolyte containing cetyltrimethylammonium chloride as a surfactant. Hexagonal array: pitch 5 μm. Pore depth 213 μm. Reproduced by permission of the Electrochemical Society.

Prepatterning has been made by pre-etching pyramidal etch pits arranged in a regular array [5,37,38]. This pre-etching was done by masking the Si surface with silicon oxide or nitride and conventional lithography, and exposing the masked surface to hot KOH solution. Nucleation of the macropores starts at the preetched pits. Perfectly regular growth can be achieved if the pitch of the nucleation array matches the average pore spacing in the conditions chosen for the anodization. If there is a significant mismatch between the prepatterning and the spontaneous pore spacing, the growth will be unstable. If the prepatterned pitch is too small, some pores will die so that the surviving ones can grow with their spontaneous spacing. If the prepatterned pitch is too large, extra pores will tend to appear between the prepatterned areas [38]. The matching condition, however, does not appear too stringent, and regular arrays of macropores have successfully been grown on p-Si. An example of such a growth is shown in Figure 2.12 [37]. Note that here the quality of pore growth was improved by the use of a cationic surfactant, an effect discussed in Section 2.4.3. Ordered arrays have been grown with a pitch of 5 μm and macropore aspect ratios of up to 100. In principle, the lower bound of the pitch size that can be realized is just limited by the size of the space charge, that is, by the lower bound of p-Si resistivity for which macropores can be grown. It is our prediction that any further increase of the band bending (by the adsorption of cationic species or the use of a suitable solvent), would be beneficial for extending this limit.

2.6. CONCLUSION

Though macropore growth on p-Si has appeared years after the corresponding studies started on n-Si, it seems to have reached a fair level of control and understanding. In general, crystallographic effects appear somewhat less marked for p-Si than for n-Si.

However, strongly anisotropic pore growth may be obtained in suitable non-aqueous solvents. Although macropores, in p-Si as well as in n-Si, do not exhibit spontaneous long-range ordering, they can be grown as long-range ordered arrays if the growth is initiated by prepatterning. Especially, the possibility to grow structures down to lower and lower resistivities may lead one to obtain smaller structures from p-Si than from n-Si. This opens the way to a variety of applications, from the manufacturing of micromechanical devices to the engineering of photonic-crystal materials.

REFERENCES

[1] R.L. Smith and S.D. Collins, J. Appl. Phys. **71**, R1–R22 (1992).
[2] L.T. Canham (Ed.), *Properties of Porous Silicon, EMIS Datareviews Series*, INSPEC, IEE, London, 1997.
[3] J.-N. Chazalviel, R.B. Wehrspohn, F. Ozanam and I. Solomon, MRS Symp. Proc. **452**, 403–414 (1997).
[4] R.B. Wehrspohn, F. Ozanam and J.-N. Chazalviel, J. Electrochem. Soc. **145**, 2958–2961 (1998).
[5] V. Lehmann and S. Rönnebeck, J. Electrochem. Soc. **146**, 2968–2975 (1999).
[6] E.K. Propst and P.A. Kohl, J. Electrochem. Soc. **141**, 1006–1013 (1994).
[7] M.M. Rieger and P.A. Kohl, J. Electrochem. Soc. **142**, 1490–1495 (1995).
[8] E.A. Ponomarev and C. Levy-Clément, Electrochemical Solid-State Lett. **1**, 42–45 (1998).
[9] E.A. Ponomarev and C. Levy-Clément, J. Porous Mater. **7**, 51–56 (2000).
[10] S. Lust and C. Levy-Clément, Phys. Status Solidi a **182**, 17–21 (2000).
[11] M. Christophersen, J. Carstensen, A. Feuerhake and H. Föll, Mater. Sci. Eng. B **69–70**, 194–198 (2000).
[12] C. Jäger, B. Finkenberger, W. Jäger, M. Christophersen, J. Carstensen and H. Föll, Mater. Sci. Eng. B **69–70**, 199–204 (2000).
[13] M. Christophersen, J. Carstensen and H. Föll, Phys. Status Solidi a **182**, 103–107 (2000).
[14] M. Christophersen, J. Carstensen, S. Rönnebeck, C. Jäger and H. Föll, J. Electrochem. Soc. **148**, E267–E275 (2001).
[15] A. Belaïdi, M. Safi, F. Ozanam, J.-N. Chazalviel and O. Gorochov, J. Electrochem. Soc. **146**, 2659–2664 (1999).
[16] J.-N. Chazalviel, M. Etman and F. Ozanam, J. Electroanal. Chem. **297**, 533–540 (1991).
[17] M. Etman, M. Neumann-Spallart, F. Ozanam and J.-N. Chazalviel, J. Electroanal. Chem. **301**, 259–265 (1991).
[18] V. Lehmann, J. Electrochem. Soc. **140**, 2836–2843 (1993).
[19] H.H. Hassan, J.L. Sculfort, M. Etman, F. Ozanam and J.-N. Chazalviel, J. Electroanal. Chem. **380**, 55–61 (1995).
[20] S. Cattarin, I. Frateur, M. Musiani and B. Tribollet, J. Electrochem. Soc. **147**, 3277–3282 (2000).
[21] J.E.A.M. Van den Meerakker and M.R.L. Mellier, J. Electrochem. Soc. **148**, G166–G171 (2001).
[22] H. Harada, T. Shirahashi, M. Nakamura, T. Ohwada, Y. Sasaki, S. Okuda and A. Hosono, Jpn. J. Appl. Phys. **40**, 4862–4863 (2001).
[23] J.-N. Chazalviel, F. Ozanam, N. Gabouze, S. Fellah and R.B. Wehrspohn, J. Electrochem. Soc. **149**, C511–C520 (2002).
[24] V. Lehmann and H. Föll, J. Electrochem. Soc. **137**, 653–659 (1990).
[25] J. Carstensen, M. Christophersen and H. Föll, Mater. Sci. Eng. B **69–70**, 23–28 (2000).
[26] W.W. Mullins and R.F. Sekerka, J. Appl. Phys. **35**, 444–451 (1964).
[27] Y. Kang and J. Jorné, J. Electrochem. Soc. **140**, 2258–2265 (1993).
[28] A. Valance, Phys. Rev. B **52**, 8323–8336 (1995).
[29] A. Valance, Phys. Rev. B **55**, 9706–9715 (1997).
[30] R.B. Wehrspohn, F. Ozanam and J.-N. Chazalviel, J. Electrochem. Soc. **146**, 3309–3314 (1999).
[31] J.-N. Chazalviel, R.B. Wehrspohn and F. Ozanam, Mater. Sci. Eng. B **69–70**, 1–10 (2000).
[32] I. Ronga, A. Bsiesy, F. Gaspard, R. Hérino, M. Ligeon, F. Muller and A. Halimaoui, J. Electrochem. Soc. **138**, 1403–1407 (1991).
[33] M. Christophersen, J. Carstensen and H. Föll, Phys. Status Solidi a **182**, 45–50 (2000).
[34] V. Lehmann and U. Gösele, Appl. Phys. Lett. **58**, 856–858 (1991).

[35] R. Memming and G. Schwandt, Surf. Sci. **4**, 109–124 (1966).
[36] E. Peiner and A. Schlachetzki, J. Electrochem. Soc. **139**, 552–557 (1992).
[37] K.J. Chao, S.C. Kao, C.M. Yang, M.S. Hseu and T.G. Tsai, Electrochem. Solid-State Lett. **3**, 489–492 (2000).
[38] A. Vyatkin, V. Starkov, V. Tzeitlin, H. Presting, J. Konle and U. König, J. Electrochem. Soc. **149**, G70–G76 (2002).